Quantifying Nerve Architecture in Murine and Human Airways Using Three-Dimensional Computational Mapping

Gregory D. Scott[1], Allison D. Fryer[1], and David B. Jacoby[1]

[1]Division of Pulmonary and Critical Care, Oregon Health and Sciences University, Portland, Oregon

The quantitative histological analysis of airway innervation using tissue sections is challenging because of the sparse and patchy distribution of nerves. Here we demonstrate a method using a computational approach to measure airway nerve architecture that will allow for more complete nerve quantification and the measurement of structural peripheral neuroplasticity in lung development and disease. We demonstrate how our computer analysis outperforms manual scoring in quantifying three-dimensional nerve branchpoints and lengths. In murine lungs, we detected airway epithelial nerves that have not been previously identified because of their patchy distribution, and we quantified their three-dimensional morphology using our computer mapping approach. Furthermore, we show the utility of this approach in bronchoscopic forceps biopsies of human airways, as well as the esophagus, colon, and skin.

Keywords: nerve; computational; modeling; neuroplasticity; three-dimensional

CLINICAL RELEVANCE

This research allows for the more comprehensive quantification of nerves and other complex linear structures in the lung, despite marked organ-wide heterogeneity. This more comprehensive quantification will improve basic and clinical studies of lung neural development and normal lung neuronal architecture, will allow for the accurate quantification of neuroplasticity in airway disease, and may provide earlier markers of disease-specific and treatment-specific neuroplasticity.

Airway nerve architecture is complex, three-dimensional, and regionally heterogeneous. It is important to measure nerve architecture accurately because it can change (structural neuroplasticity) during development or disease, resulting in altered nerve signaling. Changes in nerve structure are related to increased excitability in airway hyperreactivity, pain, itching, cardiac arrhythmias, and intestinal dysmotility (1–4), and may represent therapeutic targets in nerve lesions, heart arrhythmia, and inflammatory pain (5–8), to name a few. Changes in neuroplasticity may include swelling, central and peripheral sprouting, reduced axonal diameter, and nerve retraction. Subtler changes in nerve structure such as swelling or tortuosity may identify earlier disease time points and milder disease preceding large-scale changes in overall density (1, 9). Three-dimensional nerve architecture has been inferred from either tissue sections or from whole mounts, where data are acquired in three dimensions but are flattened to two dimensions for analysis. However, morphologically complex nerve architecture, including branching axonal processes and dendritic spines, are undersampled in two-dimensional images. Undersampling likely contributes to opposite findings of hyperinnervation and hypoinnervation in studies of asthma (10–12), diabetes (13–15), and inflammatory pain (15, 16). Design-based stereology is a newer method to reduce experimental bias (17), but objects with low sampling probability, such as airway epithelial nerve populations, require an impractical amount of sampling to fulfill the American Thoracic Society's stereology requirements for sufficient precision and efficiency (18). The limited (albeit randomized) sampling of extremely rare objects with heterogenous distributions will yield data with high variability and will require unreasonable effort to sample. Thus, all these mostly two-dimensional approaches may be inaccurate because of undersampling.

The confocal microscopy of whole mounts can image the branching structure of entire nerves, capture the organ-wide heterogeneity of nerve density, and detect low-density subpopulations. However, using confocal microscopy to model nerve architecture entails multiple problems, primarily because of tissue thickness, and even when these problems are solved, no method can currently quantify the complex three-dimensional morphology of peripheral nerves. Three-dimensional analysis is currently available for larger-scale imaging methods, such as magnetic resonance imaging (19) and X-ray computed tomography (20), and smaller-scale methods such as cryoelectron microscopy (21) and cortical fluorescence microscopy (22). Our goal involved developing an efficient method to map nerve architecture in three dimensions throughout the lung, with sufficient resolution to quantify nerve density, length, branching, and neurotransmitter content. The method we describe here can be used to image nerves throughout whole organs and tissue biopsies. A combination of adapted available computer programs with newly designed software allows for the generation of three-dimensional maps of nerve architecture that can be quantified.

MATERIALS AND METHODS

Animal and Human Tissue

Computer mapping was demonstrated for epithelial nerves in various murine tissues. Tissues were harvested from wild-type female 6- to

(*Received in original form August 1, 2012 and in final form October 2, 2013*)

This work was supported by from National Institutes of Health grants HL71795 (D.B.J.), AI92210 (D.B.J.), HL113023 (D.B.J.), AR061567 (D.B.J.), HL55543 (A.D.F.), and ES14601 (A.D.F.). G.D.S. was supported by National Institutes of Health Training Grant T32HL83808.

Correspondence and requests for reprints should be addressed to David B. Jacoby, M.D., Division of Pulmonary and Critical Care, Oregon Health and Sciences University, 3181 SW Sam Jackson Park Road, Mail Code L334, Portland, OR 97239-3098. E-mail: jacobyd@ohsu.edu

This article has an online supplement, which is accessible from this issue's table of contents at www.atsjournals.org

Am J Respir Cell Mol Biol Vol 48, Iss. 1, pp 10–16, Jan 2013

Originally Published in Press as DOI: 10.1165/rcmb.2012-0290MA on October 25, 2012
Internet address: www.atsjournals.org

8-week-old C57Bl/6 mice. Airway tissues included whole airways from the trachea to the terminal bronchioles, gastrointestinal tissues included the esophagus and descending colon, and skin was harvested from the base of the ear.

Epithelial nerves were also mapped in tracheal epithelia from guinea pigs and humans, and in airway forceps biopsies from dogs and humans. Human tracheal tissue was obtained from anonymous cadaveric organ donors via the Pacific Northwest Transplant Bank (Portland, OR). All families provided informed consent for the use of these tissues. Deidentified and fixed human airway biopsy tissues were provided by Dr. Richard Costello (Royal College of Surgeons, Dublin, Ireland), and were obtained from consenting patients with institutional approval by the Royal College of Surgeons. Pathogen-free female Dunkin-Hartley guinea pigs were obtained from Elm Hill Labs (Chelmsford, MA) in filtered crates. Canine airways were provided by the Department of Comparative Medicine at Oregon Health and Sciences University. All animals were treated in accordance with standards established by the United States Animal Welfare Act, as set forth in National Institutes of Health guidelines. All protocols involving animals were approved by the Institutional Animal Care and Use Committee of Oregon Health and Sciences University.

Tissue Dissection and Immunohistochemistry

Tissues were dissected and whole mounts were immunostained as described in the online supplement.

Generation of Deformable Surfaces for Identifying Three-Dimensional Layer Boundaries

We developed custom MatLab (Mathworks, Natick, MA) software to calculate the three-dimensional shape of each tissue layer, as detailed in the online supplement.

Diffusion Filtering to Identify Nerve Structures

For large field-of-view images, we developed diffusion filtering methods to reduce image noise and enhance nerve edges, as detailed in the online supplement.

Quantification of Nerve Structural Characteristics

For computing epithelial nerve branching and lengths from nerve maps, we used commercially available image-processing software (Imaris; Bitplane, Zurich, Switzerland). The program's image-filtering 64-bit capability and user interface allow for adaptive contour fiber tracking and the generation of tessellated nerve maps. The user defines controls points, and the computer generates three-dimensional best-fitted nerve maps to intervening image data. With nerve structures mapped, structural characteristics are quantified by the computer, including nerve lengths, branching, surface areas, and branch angles. Epithelial nerve lengths and branching were calculated for the present study and expressed in microns and number of branchpoints per 1,000 μm^3 of epithelial volume.

Comparison of Computer Nerve Mapping Analysis to Manual Human Quantification

The manual quantification of three-dimensional branchpoints and three-dimensional and two-dimensional nerve lengths was compared with three-dimensional computer nerve mapping. Three trained human observers counted branchpoints as convergences of three or more neurites or "branches," and each nerve length was calculated as the sum of Cartesian lengths for traced nerve segments, as detailed in the online supplement.

Statistical Analysis

One-way repeated-measures ANOVA with the Tukey *post hoc* test was used for nerve-mapping data. One-sample *t* tests were used for comparing manual quantifications of branchpoints and nerve lengths to the results of computer nerve mapping. Data were analyzed using GraphPad Prism 5 (GraphPad Software, La Jolla, CA).

RESULTS

Imaging Airway Innervation in Mice

Airways were imaged from the trachea to the terminal bronchioles, including the whole circumference (ventral and dorsal sides) and carina and secondary bifurcations (*see* Figure E1 in the online supplement). We acquired all images using laser scanning confocal microscopy of whole mounts. Although we also used the newer super-resolution structured illumination microscopy to acquire images, this method did not provide a practical balance of scan speed, multicolor imaging, depth resolution, and postprocessing time.

The images of nerves (labeled with protein gene product [PGP] 9.5) in airways of a whole murine lung that was also labeled with 4′,6-diamidino-2-phenylindole for cell nuclei, α–smooth muscle actin for smooth muscle, and substance P for a nerve population implicated in inflammatory disease and cough (23) are shown in Figure 1 and Video E1a in the online supplement. Whole-airway morphology can be imaged, capturing the depth from the lumen to adventitial layers, and the length from the larynx to the terminal bronchioles (Figure 1 and Videos E1a and E1b). In Figure 1 and Videos E1a and E1b, the large-scale and small-scale nerve heterogeneity (Figures 1a–1d) includes the decreased density of proximal-to-distal nerves (Figure 1a), transverse submucosal intercartilage nerves (Figures 1b and 1c), adventitial nerve bundles and ganglia (Figure 1b), undulating large-diameter nerves in smooth muscle (Figure 1c), branching small-diameter epithelial C fibers (Figure 1d), and low-density epithelial substance P nerves (Figure 1d). To quantify epithelial nerves in large field-of-view images, we developed custom software to calculate the variable three-dimensional aspects of tissue layers (Figure E2), and used image diffusion filtering to enhance nerve signals (Figure E3). We used the fiber tracking software Imaris to generate tessellated, three-dimensional maps of epithelial nerves (Figures 1e and 1f, and Video E1c).

Identification of Nerve Branching by Computational Analysis of Nerve Maps Is Superior to Manual Human Analysis

Computer analysis of the nerve maps identified more out-of-plane nerve branchpoints than did human analysis of the original images (Figures 2a–2c). Nerve branchpoints are defined as the contact points between three or more neurites. We trained volunteers in the use of the custom software, Space Software (M. Dow and G. Scott, http://lcni.uoregon.edu/∼dow/#Space_software) to rotate three-dimensional nerve images to any angle, and to identify in-plane and out-of-plane branchpoints using examples. Branchpoints were designated as "in-plane" if three branches were visible within the nonrotated image (i.e., parallel to the objective, x/y field of view, colored *red* in Figures 2a and 2b), or "out-of-plane" if at least one branch was not visible in the nonrotated image (colored *blue* in Figures 2a and 2b).

Human analysis did not find any additional branchpoints beyond those identified by computer ($n = 3$). In contrast, nerve mapping analysis by computer identified substantially more (50 versus 39.33 ± 3.0 per observer) branchpoints than did human analysis (Figure 2c). The increased branchpoints identified by computer were almost all out-of-plane, where the computer detected more than twice as many branchpoints as did humans (Figure 2c and Video E2). Computer nerve mapping showed human volunteers their missed out-of-plane branchpoints, which were subsequently confirmed by human analysis, after volunteers were shown by the computer analysis where to search. We suspect that humans missed out-of-plane branchpoints because of the amount of time and effort required to see objects that can only be visualized at one angle out of hundreds of possible angles (Video E2).

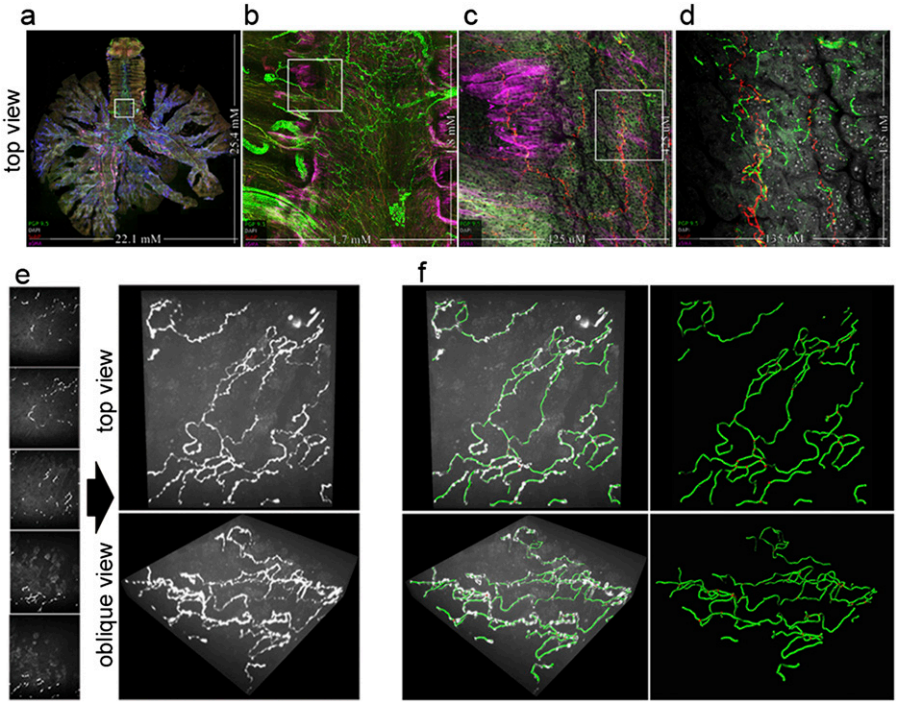

Figure 1. Whole-organ innervation and computer mapping of peripheral nerves. (*a–d*) Flattened projections of three-dimensional (3D) airway images at four magnifications capturing (*a*) whole airway innervations up to (*d*) higher-resolution epithelial nerve structure. The *boxed areas* indicate the field of view for the next panel. Nerves are labeled with a pan-neuronal antibody, PGP 9.5 (*green*). The identification of tissue compartments and subtyping nerves is demonstrated using α–smooth muscle actin (*pink*) for airway smooth muscle, 4′,6-diamidino-2-phenylindole (*white*) for cell nuclei, and substance P (*red*) for a subpopulation of sensory nerves. (*e* and *f*) Computer mapping of epithelial nerves. (*e*) Optical sectioning (z-stack) image series of airway epithelial nerves and three-dimensional visualization of images at orthogonal and oblique angles, using maximum intensity projection. (*f*) Computer nerve map (*green*) was overlaid on raw image data (*white*). After mapping, nerve structural characteristics are automatically identified and quantified. Branchpoints are shown as *red spheres*. *See* videos 1a–1c in the online supplement.

Measurement of Nerve Length Using Computational Analysis of Three-Dimensional Nerve Maps Is Superior to Manual Two-Dimensional Analysis

Nerve length was measured in nerve maps by the computer. Nerves were also manually traced by connecting line segments in three-dimensional images or in flattened two-dimensional projections of three-dimensional images, using maximum intensity projection, analogous to camera lucida tracing (Figures 2d and 2e). Nerve lengths were significantly (25.3% ± 8.8%) reduced when measured according to two-dimensional tracings of flattened images versus three-dimensional computer calculations. Nerve lengths using three-dimensional manual tracings were not significantly different from computer mapping measurements (Figure 2e), but were more labor-intense.

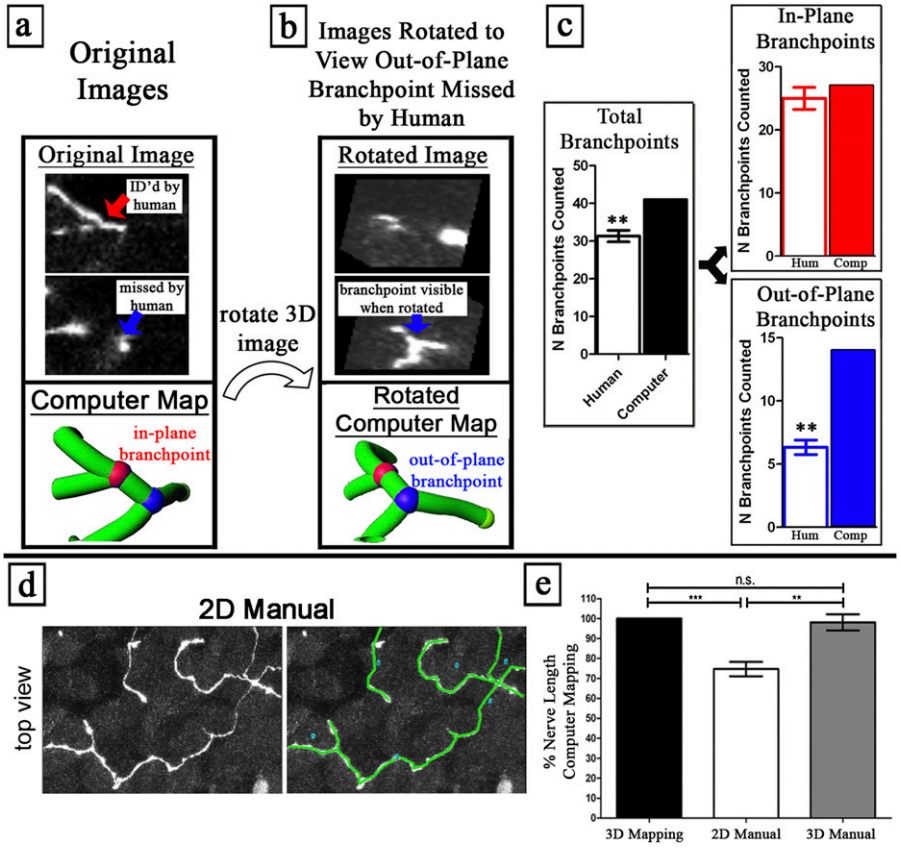

Figure 2. Computer nerve mapping identifies branchpoints and nerve lengths missed by manual analysis. (*a–c*) Out-of-plane branchpoints were identified by nerve mapping and not by manual counting. (*a*) Image slice from nonrotated ("Original Image") data contains an in-plane branchpoint (*red*), with three branches viewable in the nonrotated plane. (*b*) Image slice from rotated data ("Rotated Image") contains an out-of-plane branchpoint (*blue*), with branches oriented in a different plane from that in the original images, hence requiring image rotation to visualize. Blinded humans ($n = 3$) counted branchpoints in the same three-dimensional images. Humans were shown sample in-plane and out-of-plane branchpoints, and were taught to rotate images. (*c*) Comparison between human branchpoint counting ($n = 3$) and computer nerve mapping. Humans consistently missed out-of-plane branchpoints that computer nerve mapping correctly identified. *See* Video 2 in the online supplement. (*d–g*) A nerve length quantified using computer nerve mapping ("3D Mapping") is equivalent to the manual quantification of 3D image data ("3D Manual") and greater than the manual quantification of two-dimensional (2D) flattened image data ("2D Manual"). (*d*) Manual nerve tracing in two-dimensional and three-dimensional images. (*e*) Total nerve length was compared with computer mapping. $^{**}P < 0.01$, $^{***}P < 0.001$. n.s., no significance.

Computer Mapping Demonstrates Marked Epithelial Nerve Heterogeneity as a Function of Anatomic Location in the Airways

We demonstrated ($n = 6$ mice) that nerves are present throughout the epithelial layer of airways from the trachea to the secondary bronchi (Figure 3). Epithelial nerves exhibited a patchy distribution and complex three-dimensional morphology, with repeated branching (Figure 3a) and tortuous fiber projections between epithelial cells (Figure 1d and Videos E1a and E1b).

The quantification of nerve maps demonstrated a regional heterogeneity of epithelial nerve branches and lengths, with density decreasing markedly from the trachea to the secondary bronchi (Figure 3). Past the secondary bronchi, solitary epithelial nerves were only infrequently observed (data not shown). Within the trachea, both nerve branching and nerve length were greatest at the top of the trachea and at the dorsal midline (luminal to the trachealis muscle), and decreased both going down the trachea and moving around toward the front of the trachea (Figure 3b and Video E3a).

Decreased nerve branching was not caused by decreased nerve length for dorsal-to-lateral or dorsal-to-ventral locations, because the number of branches/unit length also decreased (Figure E4b). Furthermore, regional changes in nerve structure were not caused by changes in epithelial layer volumes, because the results did not change when ignoring epithelial volumes (Figure E5a). Both nerve lengths and nerve branching continued to decrease into the primary and secondary bronchi. A notable exception to this trend involved a dramatic increase in nerve lengths and nerve branching at airway bifurcations (i.e., at the carina and secondary bifurcation; Figure 3b).

Mapping a Low-Density, Focally Distributed Subpopulation of Murine Airway Epithelial Nerves

We mapped and quantified ($n = 6$ mice) low-density, focally distributed subpopulations of epithelial nerves in murine lungs that contained substance P (Figure E6 and Figure 4). Substance P–positive nerves accounted for 8.1% of the total nerve branchpoints and 18.4% of total neurite lengths. Similar to total nerves, as identified by PGP 9.5, substance P–containing nerves decreased progressively going down the airway from the trachea to the secondary bronchi (Figure 4 and Video E3b). However, in contrast with the total epithelial nerves, where branching and length were highest on the dorsal surface, substance P–containing nerve branching and lengths were lowest on the dorsal surface of the trachea, and increased moving ventrally (Figure 4 and Video E3b). This proximal/distal and ventral/dorsal distribution of substance P–containing nerves was evident regardless of whether branchpoints or nerve lengths were quantified, or whether data were expressed as percentages of total nerves (identified by PGP9.5 staining; Figure 4). Increased substance P nerve branching, measured dorsal to ventral, was independent of total nerve length (Figure E4d) or epithelial volume (Figure E5b). In contrast, decreased substance P nerve branching, measured proximal to distal, was dependent on nerve length (Figure E4c), but not epithelial volume (Figure E5b). Moreover, in contrast to epithelial nerves as a whole, no increase in substance P–containing nerves at airway bifurcations was evident (compare Figure 3 with Figure 4).

Clinical Potential: Mapping Human Airway Nerves

We were able to preserve the delicate epithelial nerve morphology in both human tracheas obtained at autopsy and guinea pig tracheas. We performed similar tissue preparations and analyses as in mice, with the additional step of dissecting the epithelium free of deeper tissues to reduce light absorbance/scatter during image acquisition. Nerves were stained and imaged and mapped with the computer, and their morphology was quantified. For two guinea pig tracheas, mean epithelial nerve branching comprised 81 ± 5.0 branchpoints per field, and nerve length was measured at 3,233.6 ± 254.1 μM per field (Figure E7a). In three human-autopsy tracheas, the mean epithelial nerve branching comprised 23.2 ± 22.7 branchpoints per field, and nerve length was measured

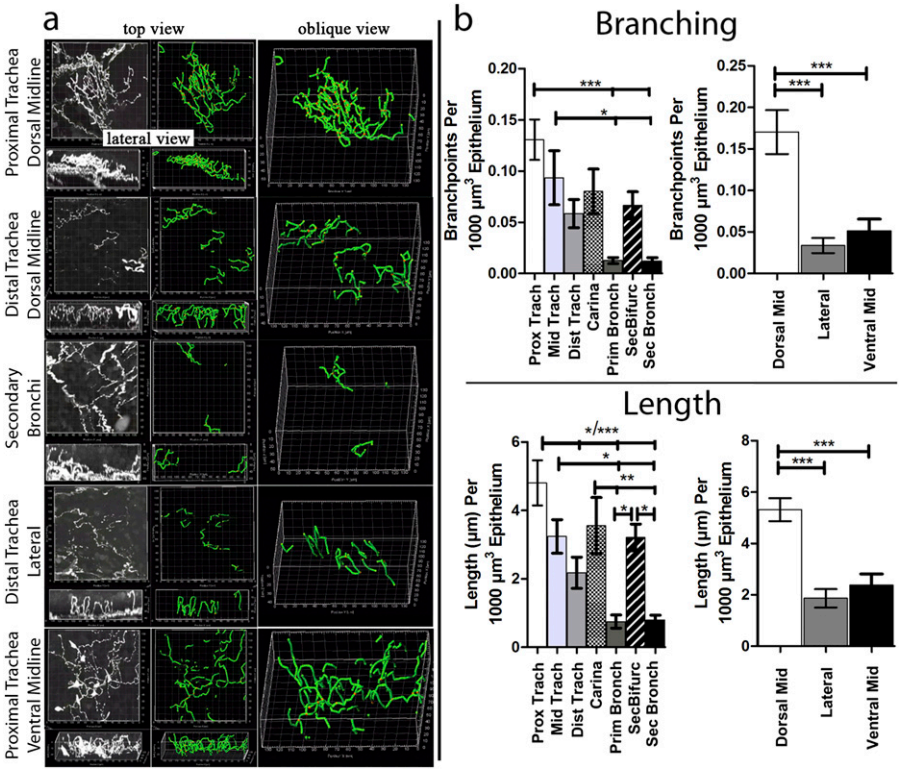

Figure 3. Organ-wide structural quantification of murine airway epithelial nerves. (*a*) Top and lateral views of epithelial nerves (*white*) in different regions of the large airways, with nerve maps (*green*) overlaid on nerve image data. *See* Figure E1 for a diagram of airway regions. (*b*) After mapping, nerve lengths and numbers of branchpoints were quantified by the computer ($n = 6$). Nerve lengths and branching decreased proximal-to-distal, with regional increases at airway bifurcations. Nerve lengths and branching decreased from the dorsal midline to lateral and ventral positions in the trachea. $^*P < 0.05$, $^{**}P < 0.01$, $^{***}P < 0.001$.

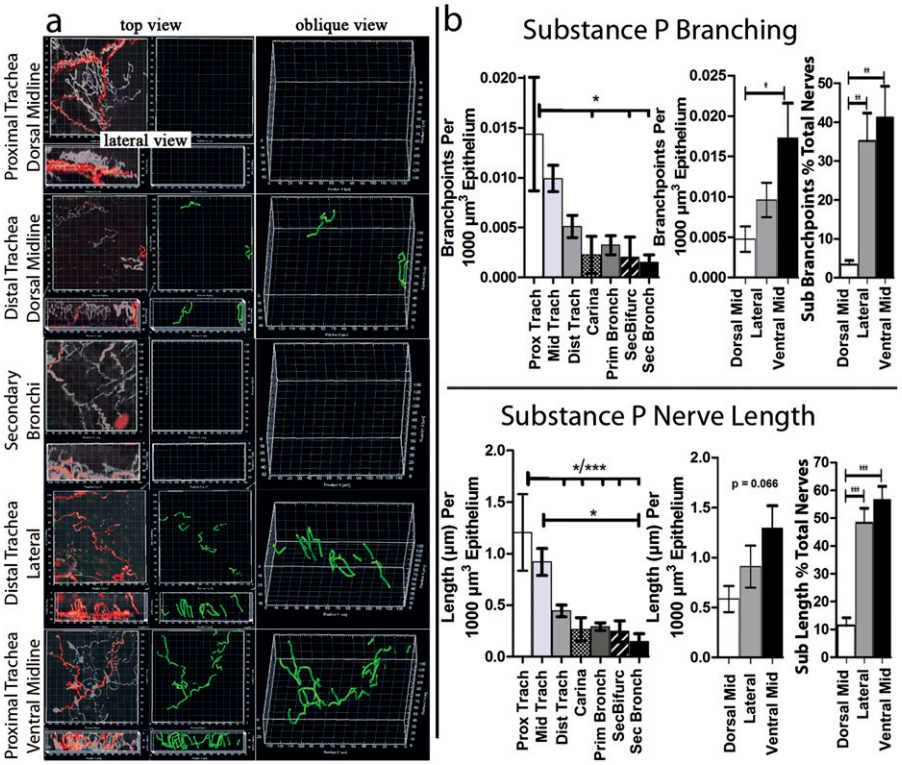

Figure 4. Distinct organ-wide structure of an airway epithelial nerve subpopulation. (*a*) Top and lateral views of substance P–expressing nerves (*red*) were overlaid on nerves labeled with a pan-neuronal marker (*white* to *transparent*). Computer substance P nerve map (*green*) was overlaid on image data. (*b*) After mapping, epithelial substance P nerve lengths and branching were quantified by the computer ($n = 6$). Unlike total epithelial nerves identified by PGP 9.5, substance P nerve lengths and branching increased from dorsal to lateral and ventral positions. This incrase was also seen when substance P nerve lengths and branching were calculated as percentages of total nerve lengths and branching. Unlike total nerves, substance P nerve lengths and branching did not increase at airway bifurcations. $^*P < 0.05$, $^{**}P < 0.01$, $^{***}P < 0.001$. *See* Figure E1 for a diagram of the airway region.

at 1,915.2 ± 1,127.4 μM per field (Figures 5a and 5b and Videos E4a and E4b). Although these data appear to demonstrate that the nerves were less dense, in terms of both branching and length, in human tracheas than in guinea pig tracheas, more variability was evident in the human tracheas, and thus additional data would be required before a species comparison could be performed.

Because airway tissues from living humans are predominantly obtained by bronchoscopy using endobronchial biopsy forceps and are typically only approximately 1 mm in diameter, to determine whether we could image nerves in such biopsies was important. These biopsies could also be crushed or the epithelium abraded, both of which could damage nerve architecture. We initially demonstrated that nerve architecture was preserved and quantifiable in forceps biopsies from an otherwise discarded dog airway (Figure E7b). Bronchoscopic forceps biopsies obtained from human volunteers also showed quantifiable nerve architecture in biopsies taken from the carina and from the secondary bifurcation of the airways (Videos E4c and E4d). The innervation of columnar and squamous epithelia in biopsy tissue specimens is demonstrated in Figures 5c and 5d, respectively.

Application in Skin, Esophagus, and Intestine

The nerve supply is unique in each organ system. To test whether we could quantify the nerve architecture in organs outside the lungs, we mapped epithelial nerves in murine skin, esophagus, and colons. Similar to the airways, the nerve morphology was preserved and quantifiable. In skin (Figure E8a), epithelial nerve branching comprised 167 ± 43.8 branchpoints per field, and the nerve length was measured at 3,356.6 ± 699.4 μM per field ($n = 8$; 5 replicates/mouse). In the esophagus (Figure E8b) and colon (Figure E8c), we counted 72 and 166 branchpoints, respectively, and nerve length was measured at 1,659.7 μM and 3,564.4 μM per field, respectively ($n = 1$).

Mapping the Substance P Subpopulation of Epithelial Nerves in Human Tissues and Other Organs

Using this method, we were also able to detect and map substance P–containing nerves in human airway biopsies (Figure E9b and Videos E4c and E4d), human autopsy tracheas (Figure E10), guinea pig airways (Figure E9a), and murine skin (Figure E9c).

DISCUSSION

Nerves are capable of exhibiting an array of rapid and long-term structural changes, including nerve swelling, fragmentation, retraction, growth, and branching (24, 25). Previous work has shown that in disease, structural neuroplasticity coincides with functional neuroplasticity (1, 13, 26). Human studies have linked increased nerve density to cough (27), cardiac arrhythmias (28), and inflammatory pain (16), to name a few conditions. However, our ability to measure these changes has been hindered by a limited view of individual nerve morphologies.

We mapped airway epithelial nerves to demonstrate the quantification of fine nerve architecture in the context of organ-wide heterogeneity. We used whole-mount confocal microscopy and computer mapping because they captured more nerve structural information compared with traditional two-dimensional methods. We detected a heterogeneous distribution of epithelial nerves throughout the large airways, although epithelial nerves in mice were previously thought either not to exist, or to supply only neuroepithelial cells (29, 30). We found that the distribution of epithelial nerves fluctuates, with dense patches near airway bifurcations, and decreases in average nerve lengths and branching distally. A map that includes both fine nerve architecture and organ-wide distribution has not been previously created. The heterogeneity of epithelial nerve density may be anatomically important for sensing inhaled particles, because nerve distribution is remarkably similar to inhalant deposition patterns (31). This sparse distribution and complex branching morphology would likely have been undersampled by two-dimensional methods. Our results show that two-dimensional image flattening leads to underestimations of nerve length and branching, particularly when nerves and branches are oriented out-of-plane in the z direction.

We further tested the sensitivity of this method by imaging the sparse subpopulation of epithelial nerves that contain substance P.

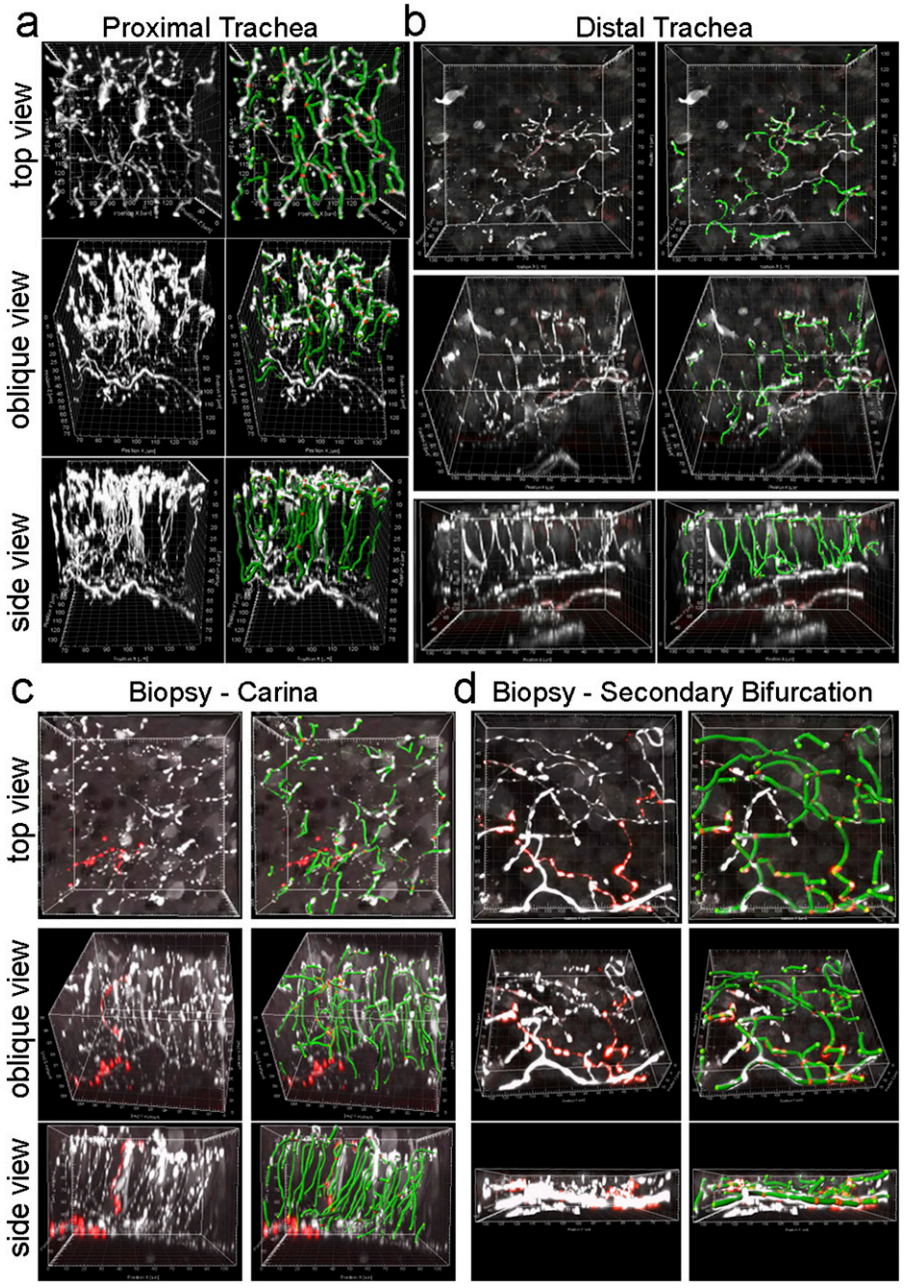

Figure 5. Epithelial nerve mapping in human airway tissue. (*a* and *b*) Top, oblique, and lateral projections of human epithelial nerves (*white*) in the proximal and distal trachea were overlaid with computer nerve maps (*green*, with *red spheres* as branchpoints). (*c* and *d*) Epithelial nerves and nerve mapping in airway forceps biopsy tissue from airway bifurcations. Columnar epithelium was present in the trachea autopsy specimens and carina biopsy specimen. Squamous epithelium was present in the secondary bifurcation biopsy specimen. Substance P epithelial nerves (*red*) are shown in *c* and *d*.

In the lungs, this subset of afferent C-fibers is associated with the symptoms of asthma and with neurogenic inflammation (32, 33). Our data showed a dorsal-to-ventral distribution of substance P–expressing epithelial nerves that was opposite to the distribution of all epithelial nerves. This demonstrates how nerve distribution, as a whole, is not necessarily predictive of the distribution of individual subpopulations, and requires a sensitive technique for purposes of study. Substance P nerves were heterogeneous and present at low density (only 8% of branchpoints were substance P–positive), and thus an impractically large number of tissue sections would have been necessary to capture substance P–positive epithelial nerve distribution.

We have also shown that in biopsy specimens, this method will keep three-dimensional nerve morphology intact, and can quantify nerve architecture. Clinical studies in living patients require the use of biopsies from the airways, skin, and intestine. Fiberoptic bronchoscopy with endobronchial forceps biopsy allows for the quantification of nerves before and after any treatment, and also allows for the correlation of nerve quantification with disease (as assessed by clinical findings or laboratory tests). Our method contains a major advantage, namely, by not sectioning the tissue or flattening nerve images, we are able to see all nerves in the biopsy, thus drastically reducing undersampling. Our method was also sensitive enough to identify substance P–positive nerves consistently in human biopsy specimens, whereas some studies using tissue sections could not identify substance P–containing nerves (11). We also demonstrated the feasibility of our approach to quantify nerves in other organs, including the skin, esophagus, and colon. Organ-wide quantification will be important for future studies of these organs, because nerves in the gastrointestinal system and skin are known to be highly heterogenous. The colon contains a patchwork of hypoganglionic regions surrounded by dense nerve clusters (34), whereas nerve density in human skin can vary by up to 50%, depending upon a patient's age and skin region (35).

Overall, our technique is applicable to the preclinical and clinical research of disease and developmental structural changes to peripheral nerves. We expect newer image analysis techniques to resolve the widespread conflicts in disease neuroplasticity studies (10–16), to quantify early subtler changes in nerve architecture that precede changes in overall density (1, 9), and to advance studies of neuroplasticity as a therapeutic target (5–8).

Author disclosures are available with the text of this article at www.atsjournals.org.

Acknowledgments: The authors thank the members of the Pacific Northwest Transplant Bank for their help in procuring human tracheas. The authors also thank Dr. Richard Costello of the Royal College of Surgeons (Dublin, Ireland) for bronchoscopic biopsies from human subjects.

References

1. Lauria G, Cornblath DR, Johansson O, McArthur JC, Mellgren SI, Nolano M, Rosenberg N, Sommer C; European Federation of Neurological Surgeons. EFNS guidelines on the use of skin biopsy in the diagnosis of peripheral neuropathy. *Eur J Neurol* 2005;12:747–758.
2. Grossmann L, Gorodetskaya N, Teliban A, Baron R, Janig W. Cutaneous afferent C-fibers regenerating along the distal nerve stump after crush lesion show two types of cold sensitivity. *Eur J Pain* 2009; 13:682–690.
3. Janig W, Grossmann L, Gorodetskaya N. Mechano- and thermosensitivity of regenerating cutaneous afferent nerve fibers. *Exp Brain Res* 2009;196:101–114.
4. Janse C, Peretz B, van der Roest M, Dubelaar EJ. Excitability and branching of neuroendocrine cells during reproductive senescence. *Neurobiol Aging* 1999;20:675–683.
5. Beirowski B, Nogradi A, Babetto E, Garcia-Alias G, Coleman MP. Mechanisms of axonal spheroid formation in central nervous system wallerian degeneration. *J Neuropathol Exp Neurol* 2010;69:455–472.
6. Terada M, Yasuda H, Kikkawa R. Delayed wallerian degeneration and increased neurofilament phosphorylation in sciatic nerves of rats with streptozocin-induced diabetes. *J Neurol Sci* 1998;155:23–30.
7. Wernli G, Hasan W, Bhattacherjee A, van Rooijen N, Smith PG. Macrophage depletion suppresses sympathetic hyperinnervation following myocardial infarction. *Basic Res Cardiol* 2009;104:681–693.
8. Woolf CJ. Phenotypic modification of primary sensory neurons: the role of nerve growth factor in the production of persistent pain. *Philos Trans R Soc Lond B Biol Sci* 1996;351:441–448.
9. Kallinikos P, Berhanu M, O'Donnell C, Boulton AJ, Efron N, Malik RA. Corneal nerve tortuosity in diabetic patients with neuropathy. *Invest Ophthalmol Vis Sci* 2004;45:418–422.
10. Ollerenshaw SL, Jarvis D, Sullivan CE, Woolcock AJ. Substance P immunoreactive nerves in airways from asthmatics and nonasthmatics. *Eur Respir J* 1991;4:673–682.
11. Howarth PH, Springall DR, Redington AE, Djukanovic R, Holgate ST, Polak JM. Neuropeptide-containing nerves in endobronchial biopsies from asthmatic and nonasthmatic subjects. *Am J Respir Cell Mol Biol* 1995;13:288–296.
12. Goldie RG, Fernandes LB, Rigsby PJ, Pudney CJ, Spalding LJ, O'Connor BJ, Page CP. Airway structure: a role for confocal microscopy? *Pulm Pharmacol Ther* 1998;11:349–354.
13. Di Giulio AM, Tenconi B, La Croix R, Mantegazza P, Abbracchio MP, Cattabeni F, Gorio A. Denervation and hyperinnervation in the nervous system of diabetic animals: II. Monoaminergic and peptidergic alterations in the diabetic encephalopathy. *J Neurosci Res* 1989;24:362–368.
14. Sharma AK, Thomas PK. Peripheral nerve structure and function in experimental diabetes. *J Neurol Sci* 1974;23:1–15.
15. Sorensen L, Molyneaux L, Yue DK. The relationship among pain, sensory loss, and small nerve fibers in diabetes. *Diabetes Care* 2006;29: 883–887.
16. Fitzgerald M, Beggs S. The neurobiology of pain: developmental aspects. *Neuroscientist* 2001;7:246–257.
17. Hyde DM, Harkema JR, Tyler NK, Plopper CG. Design-based sampling and quantitation of the respiratory airways. *Toxicol Pathol* 2006;34: 286–295.
18. Hsia CC, Hyde DM, Ochs M, Weibel ER. Structure AEJTFoQAoL: an official research policy statement of the American Thoracic Society/ European Respiratory Society: standards for quantitative assessment of lung structure. *Am J Respir Crit Care Med* 2010;181:394–418.
19. Manniesing R, Viergever MA, Niessen WJ. Vessel enhancing diffusion: a scale space representation of vessel structures. *Med Image Anal* 2006;10:815–825.
20. Bauer C, Pock T, Sorantin E, Bischof H, Beichel R. Segmentation of interwoven 3D tubular tree structures utilizing shape priors and graph cuts. *Med Image Anal* 2010;14:172–184.
21. Jiang M, Ji Q, McEwen BF. Model-based automated extraction of microtubules from electron tomography volume. *IEEE Trans Info Technol Biomed* 2006;10:608–617.
22. Lindquist BW, Koh IYY, Weaver CM. 3DMA-neuron: a software package for automated neuronal morphology. 1999 accessed September 9, 2011]. Available from: http://www.ams.sunysb.edu/∼lindquis/3dma/3dma_neuron/3dma_neuron.html.
23. Barnes PJ, Chung KF, Page CP. Inflammatory mediators of asthma: an update. *Pharmacol Rev* 1998;50:515–596.
24. Chakrabarty A, McCarson KE, Smith PG. Hypersensitivity and hyperinnervation of the rat hind paw following carrageenan-induced inflammation. *Neurosci Lett* 2011;495:67–71.
25. Kerschensteiner M, Schwab ME, Lichtman JW, Misgeld T. *In vivo* imaging of axonal degeneration and regeneration in the injured spinal cord. *Nat Med* 2005;11:572–577.
26. Oh YS, Jong AY, Kim DT, Li H, Wang C, Zemljic-Harpf A, Ross RS, Fishbein MC, Chen PS, Chen LS. Spatial distribution of nerve sprouting after myocardial infarction in mice. *Heart Rhythm* 2006;3: 728–736.
27. O'Connell F, Springall DR, Moradoghli-Haftvani A, Krausz T, Price D, Fuller RW, Polak JM, Pride NB. Abnormal intraepithelial airway nerves in persistent unexplained cough? *Am J Respir Crit Care Med* 1995;152:2068–2075.
28. Cao JM, Fishbein MC, Han JB, Lai WW, Lai AC, Wu TJ, Czer L, Wolf PL, Denton TA, Shintaku IP, *et al*. Relationship between regional cardiac hyperinnervation and ventricular arrhythmia. *Circulation* 2000;101:1960–1969.
29. Adriaensen D, Brouns I, Van Genechten J, Timmermans JP. Functional morphology of pulmonary neuroepithelial bodies: extremely complex airway receptors. *Anat Rec A Discov Mol Cell Evol Biol* 2003;270:25–40.
30. Karlsson JA, Sant'Ambrogio G, Widdicombe J. Afferent neural pathways in cough and reflex bronchoconstriction. *J Appl Physiol* 1988;65: 1007–1023.
31. Lambert AR, O'Shaughnessy P, Tawhai MH, Hoffman EA, Lin CL. Regional deposition of particles in an image-based airway model: large-eddy simulation and left-right lung ventilation asymmetry. *Aerosol Sci Technol* 2011;45:11–25.
32. Canning BJ, Chou YL. Cough sensors: I. Physiological and pharmacological properties of the afferent nerves regulating cough. *Handb Exp Pharmacol* 2009;187:23–47.
33. Groneberg DA, Quarcoo D, Frossard N, Fischer A. Neurogenic mechanisms in bronchial inflammatory diseases. *Allergy* 2004;59:1139–1152.
34. Sibaev A, Franck H, Vanderwinden JM, Allescher HD, Storr M. Structural differences in the enteric neural network in murine colon: impact on electrophysiology. *Am J Physiol Gastrointest Liver Physiol* 2003;285:G1325–G1334.
35. McArthur JC, Stocks EA, Hauer P, Cornblath DR, Griffin JW. Epidermal nerve fiber density: normative reference range and diagnostic efficiency. *Arch Neurol* 1998;55:1513–1520.